Laboratoire Jacques-Louis Lions
Sorbonne Université

Master 2 Internship report
Mathematics and applications

Modeling intratumoral cellular interactions in oral cavity cancers

AUTHOR
Sela Lia

ADVISORS
Emmanuel Trélat and Jean Clairambault

ACADEMIC YEAR 2024

Contents

Acknowledgements

I would like to express my sincerest gratitude to everyone who guided me through this internship.

Primarily I am deeply grateful to my advisors Jean Clairambault and Emmanuel Trélat for their indispensable support through this internship. I want to thank them for letting me work on this captivating subject they designed and for their considerable help along the internship.

I am also very thankful to Frank Ernesto Alvarez who dedicated time and was very kind to answer my questions and raise my curiosity. I would like to thank Camille Pouchol as well for giving me the opportunity to exchange with him and learn from his great knowledge on the subject.

A special thanks to the medical researcher Jean-Phillipe Foy for showing great interest in this work. This remarkable collaboration between mathematics and oncology presents a unique opportunity to gain a profound understanding of the mechanisms. His guidance thus allows us to find direct applications to our research by specifying currently relevant clinical issues that can be addressed through modeling.

Finally, I feel grateful for my friends and family for their encouragement and their company all along these months.

Introduction

This internship report provides an overview of the work carried out over a four-month internship at the Jacques-Louis Lions Laboratory (LJLL) during spring 2024. It is essentially an introduction to the numerical and mathematical modelling of cells interactions in cancer, with the intention to establish an appropriate framework for the PhD following this internship, titled ”Modeling cellular phenotypic divergence in oral carcinogenesis to improve oral cavity cancer prevention and treatment”. This subject was designed during the internship, thanks to the fruitful collaboration between my advisors Jean Clairambault and Emmanuel Trélat and the medical researcher Jean-Phillipe Foy.

This report will be structured in two independent sections. In the first part, we shall detail the biological context and the considerations that helped set up the models. The second part will be dedicated to a mathematical and numerical analysis of the models, and to a description of some first results on numerical therapeutic optimal control.

Chapter 1

Biological background and modeling

In this chapter, we will investigate the biology of oral cancer with the aim of developing mathematical models adapted to answer specific contemporary challenges. Understanding the biological mechanisms driving carcinogenesis is crucial for constructing accurate and effective mathematical models.

The ongoing biological questions raised by medical researchers will serve as a foundation for our mathematical and numerical modeling, with the goal of a better understanding of cancer dynamics and an improvement of therapeutic strategies.

1.1 Oral cancers

1.1.1 A general overview

Oral cavity cancers are the most frequent cancer types (35%[1]) within head and neck cancers and arise in the mouth, the lips, and the upper throat. The most common histological type (95%[1]) and the one we will be focusing on is oral squamous cell carcinoma (OSCC), which is linked to considerable morbidity and mortality.

OSCC originates in the epithelial cells of the mucosal linings, which suggests that it is a rather homogeneous disease, as it develops from one cell type in one tissue. The biological reality is that OSCC is remarkably heterogeneous due to the complexity of the anatomical structures concerned as well as the diversity of the molecular changes taking place during carcinogenesis [2].

The importance of the immune micro-environment in oral carcinogenesis has recently gained strength. The tumor micro-environment refers to the wide variety of malignant and non-malignant cell populations surrounding the tumor and to the molecules they produce. In this study, we shall concentrate our investigation towards the dynamics between immune cells and cancerous cells during oral carcinogenesis. The infiltration of various immune cell types has been analyzed, along with their positive and negative effects on cancer development. In [3] a deconvolution of the different

immune cell types was performed. Figure 1.1 presents the relative percentages of each immune cell type across the 4 identified steps of oral carcinogenesis: normal stage, hyperplasia (excessive cell proliferation), dysplasia (loss of healthy characteristics) and carcinoma.

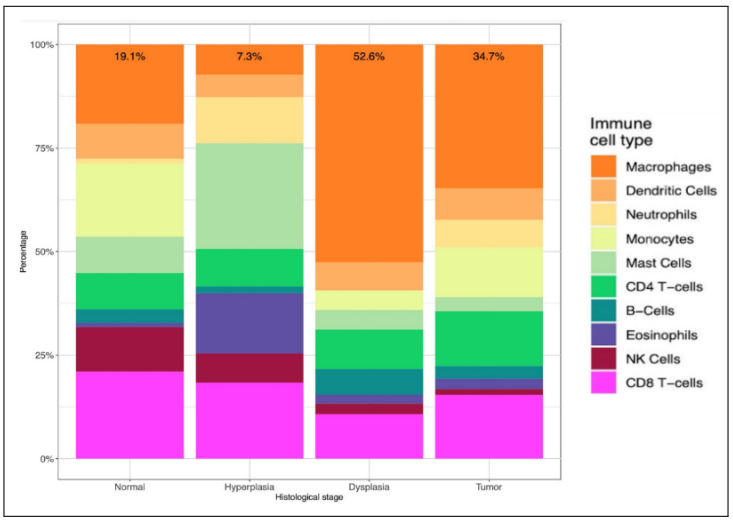

Figure 1.1: Deconvolution of immune cell populations in murine stroma samples

It appears that macrophagic infiltration plays an important role especially during dysplasia. Yet the role of the macrophages remains poorly understood. Macrophages are immune cells involved in the immune response classified in two groups : M1 and M2 -although recent studies have identified a wide variety of macrophages subsets [4]. Macrophages have the ability to switch their phenotype towards M1 or M2 depending on the neighboring environment. They also play an active role in cancer progression. As a matter of fact it is commonly believed that M2 macrophages have a protumorigenic action on developed tumors. However in [3], Jean-Phillipe Foy and his collaborators unexpectedly found a positive correlation between M2 macrophages signature expression and oral cancer-free survival of patients with precancerous lesions, as illustrated in Figure 1.2. This recent discovery suggests that the role of M2 macrophages fluctuates in oral cancers. A major stake is thus identifying the factors that lead M2 macrophages to have a pro or anti-tumorigenic action.

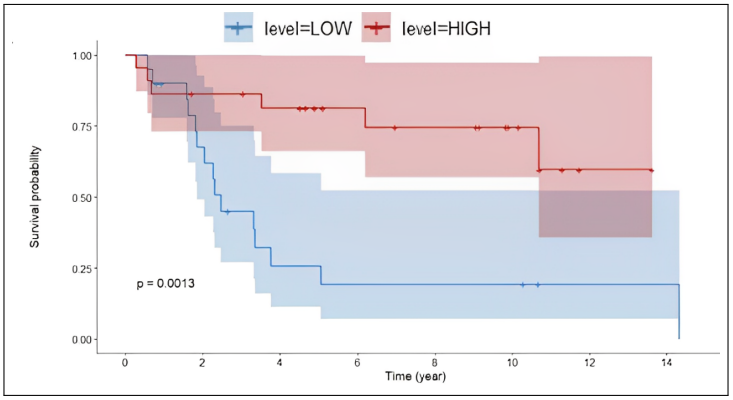

Figure 1.2: Association of M2 macrophages gene expression signature with oral cancer-free survival

1.1.2 Clinical issues

The main risk factors of oral cavity cancers are tobacco and excessive alcohol use. The combined use of tobacco and alcohol further increases the risk. Here the clinical concern we will focus on is precancerous lesions. Around 20% of OSCC appear from precancerous lesions [5]. Such precancerous lesions also called oral potentially malignant disorders are chronic diseases of the oral mucosa characterized by a greater than normal risk of malignancy. These lesions are visible to the naked eye and can appear as white (leukoplakia) or red (erythroplakia) patches.

OSCC carcinogenesis involves a multi-stage process associated to genetic and epigenetic changes whereby the normal oral epithelium transforms into a malignant state. The different steps are review in Figure 1.3.

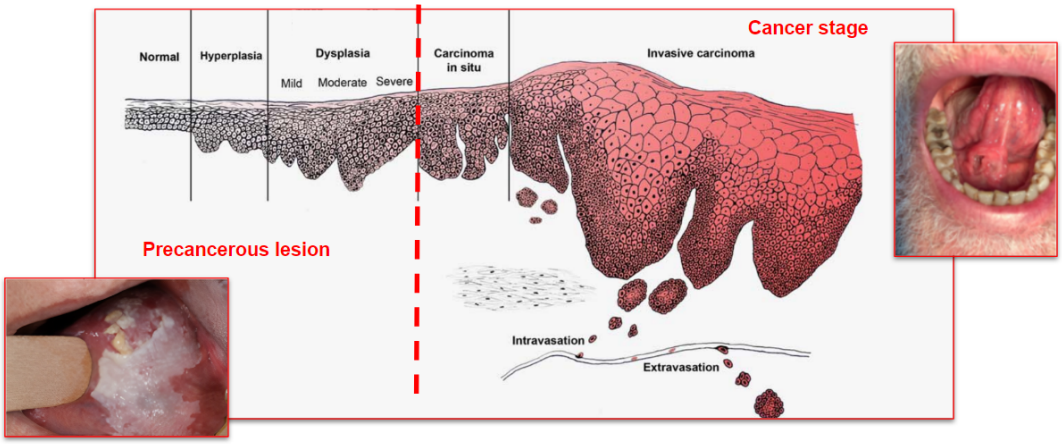

Figure 1.3: Multi-step carcinogenesis model [6]

As not all lesions have the same risk of malignant transformation, one of the primary clinical concerns is to develop strategies that can help determine the likelihood that a lesion will progress to a cancerous stage as well as prevent a cancerous transformation of these lesions. A better targeting of the patients could help reduce the costs raised by prevention therapies and prevent risk-free patients from undergoing heavy treatments.

1.1.3 Immunotherapies

The most widely used treatment to cure cancer is chemotherapy, but it is becoming more and more limited due to its side effects and to drug resistance. For this reason current oncology research is shifting towards other therapeutic strategies such as immunotherapies.

A promising therapeutic research direction to prevent the development of cancerous tissues from oral potentially malignant disorders in the oral cavity is the use of immune checkpoint inhibitors. Checkpoints inhibitors are a normal component of the immune system that play a key role in restraining the immune response from being too vigorous.

Notably the PD-1/PD-L1 pathway holds promising applications for the treatment of oral cancers. Programmed Cell Death Protein 1 (PD-1) is a protein found on the surface of T cells modulating their activity. Programmed Cell Death Ligand 1 (PD-L1) is a protein that can be produced by tumors to bind to PD-1, thereby preventing cancerous cells from being killed by the immune response. This mechanism, known as cancer immune escape, is one of the hallmarks of cancer [7]. Anti-PD-1 or anti-PD-L1 immunotherapy drugs act by blocking the pathway PD-1/PD-L1 allowing to remove the inactivation of the immune system by cancerous cells.

However an approved approach to prevent the malignant transformation of precancerous lesions have not been established so far [3] and immunotherapies are not yet in use to treat OSCC in France. The use of mathematical modeling should provide a better understanding of the dynamics involved in immunotherapies.

1.2 Mathematical modeling of cell populations dynamics in cancer

1.2.1 Outline

Understanding early cancer development as well as immune infiltration, in particular macrophages infiltration in cancerous tissues is a very complex process. Mathematical modelling seems to be an adapted and efficient tool that can help apprehend these complex biological mechanisms and has been widely used in similar contexts, see [8], [9] and [10].

Mathematical modeling with partial differential equations (PDE) structured in continuous phenotypes appears to be perfectly adapted for our study. As a matter of fact we will put our focus on the cellular phenotypic changes that drives the carcinogenesis. The continuous property of phenotypes seems to fit with the recent observations according to which the macrophage switch is continuous and reversible.

In order to investigate the role of macrophagic infiltration in OSCC we will focus on modelling the interactions between two cellular populations : one macrophagic population and one epithelial population susceptible of having cancerous behavior. We will be interested by studying the co-evolution of the two populations over time depending on the evolutions of their phenotypes. The long term purpose is then to clarify the role of M1 and M2 macrophages during carcinogenesis by understanding the dynamics observed through the biological data.

1.2.2 Biological data

In the long term, the objective is to refine the models developed in this report using biological data derived from both murine and human studies conducted by Jean Phillipe Foy and his collaborators.

The biological data and more broadly the bibliography on the subject is also necessary to settle valid modeling hypotheses before going through the mathematical analysis of the models. It is not the focus of this report, as we will primarily introduce generic models that will need further refinement to align with biological reality.

The data already available notably used in [3] consists of few sets containing the RNA expression of more than 20 000 genes during the different phases of murine carcinogenesis : normal stage, hyperplasia, dysplasia, and malignity. From this raw data it is possible to extract enrichment scores of biologic cellular pathways or cell population types, using previously established signatures. For instance we can calculate the enrichment score of apoptosis to provide an accurate estimation of the death terms involved in our equations displayed further on, or the enrichment score of M2 macrophages to compare with the models prediction and make adjustments.

This will enhance the accuracy and relevance of our mathematical models ensuring they are able to answer the previously depicted challenges in OSCC research. By integrating detailed experimental data we aim to achieve a deeper understanding of the biological processes at play, ultimately leading to improved predictive capabilities and therapeutic strategies.

Chapter 2

Mathematical and numerical modeling

2.1 Introduction to the model

We consider a system of two cellular populations interacting with each other : a macrophagic population M and an epithelial population E. The typical equations used in similar contexts are non-local integro-differential equations coming from adaptive dynamics.

We denote $n_M(t,x)$ the density of the macrophage population of phenotype x at time t and $n_E(t,y)$ the density of the epithelial population E of phenotype y at time t.

To keep things simple the phenotypes x and y will be in this section uni-dimensional, taking values in $[0,1]$.

- For macrophage cells, x ranges from 0 for an M1 phenotype to 1 for a M2 phenotype.
- For epithelial cells, y ranges from 0 for a weak differentiation potential (very specialized cell) to 1 for a strong differentiation potential (close to stem cell properties).

We consider the following two-dimensional system of partial differential equations:

$$\begin{cases} \partial_t n_M(t,x) = n_M(t,x)\ [r_M(x) - d_M(x)\rho_M(t) + \rho_E(t)\phi_M(t)] & (t,x) \in [0,\infty) \times [0,1] \\ \partial_t n_E(t,y) = n_E(t,y)\ \ [r_E(y) - d_E(y)\rho_E(t) + \rho_M(t)\phi_E(t)] & (t,y) \in [0,\infty) \times [0,1] \end{cases} \tag{2.1}$$

Each term describes a separate phenomenon, for $C \in \{M,E\}$ and $z \in \{x,y\}$ we have:

- The birth rate of population C: $r_C(z)$ as a function of the phenotype z.
- The death term of population C: $d_C(z)\rho_C(t)$ where the death rate is $d_C(z)$ and the total mass is denoted :

$$\rho_C(t) := \int_{[0,1]} n_C(t,w)dw.$$

- For $D \in \{M, E\}, D \neq C$, the action of population D on population C is represented by the term $\rho_D(t)\phi_C(t)$. The underlying assumption is that this action is proportional to the total mass of population D and depends more specifically on the population C through the function ϕ_C. This notation must be used with caution: ϕ_C can and will explicitly depend on n_C.

  One typical way of choosing ϕ_C is to define:

$$\phi_C(t) = \int_{[0,1]} \psi_C(z) n_C(t,z) dz \quad \forall t \in [0, \infty).$$

  $\psi_C(z)$ is here a weight function quantifying the effectiveness of the interaction as a function of the phenotype. Its sign gives precious knowledge about the nature of interactions between the two populations : mutualistic (if positive) or competitive (if negative). Along this report we will mainly focus on mutualistic interactions but a long term objective is to apprehend the case when the sign of ψ_C is fluctuating, which appears to be closer the the biological reality as explained in section 1.1.1.

In order to delve deeper into the subject we expect in the long term more accurate information on the dependency of r and ϕ on the phenotypes from our medical collaborator Jean-Phillipe Foy. While waiting for such material we shall here explore the possible representations of these interactions through trial and error.

2.2 Mathematical analysis

2.2.1 One population

For a better understanding of the system, let us first focus on the single population case. We consider one partial differential equation describing the temporal evolution of one cell population.

Our modeling assumption is that the birth and death rate are positive constants respectively equal to r and d. The non local integro-differential equation characterizing the evolution of the density is then:

$$\begin{cases} \partial_t n(t,x) = n(t,x)(r - d\rho(t)), & (t,x) \in [0,\infty) \times [0,1] \\ n(0,x) = n^0(x), & x \in [0,1] \end{cases} \tag{2.2}$$

where $\rho(t) := \int_{[0,1]} n(t,z)dz$ and $n^0 \in C([0,1])$.

Integrating (2.2) over $[0,1]$, one gets:

$$\begin{cases} \rho'(t) = \rho(t)(r - d\rho(t)) & t \in [0,\infty) \\ \rho(0) = \int_{[0,1]} n^0(z)dz := \rho_0 \end{cases} \tag{2.3}$$

Lemma 1. The unique solution of (2.3) on $[0, \infty)$ is:

$$\bar{\rho}(t) = \frac{r\rho_0 e^{rt}}{r - d\rho_0 + d\rho_0 e^{rt}}$$

Proof. Direct calculations show that $\bar{\rho}$ is a solution of (2.3). The uniqueness comes from the Cauchy Lipschitz theorem. □

Proposition 1. There exists a unique solution to (2.2) on $[0, \infty) \times [0, 1]$ for which we have the explicit formula:

$$\bar{n}(t, x) = \frac{re^{rt}}{r - d\rho_0 + d\rho_0 e^{rt}} n^0(x)$$

Proof. As $\bar{n}(t, x) = \frac{\bar{\rho}(t)}{\rho_0} n^0(x)$, we have $\partial_t \bar{n}(t, x) = \frac{\rho'(t)}{\rho_0} n^0(x)$ so from **Lemma 1** we have that $\bar{n}(t, x)$ is a solution of (2.2).

For the uniqueness, we rewrite (2.2) as a local system:

$$\frac{d}{dt} \begin{pmatrix} n(t, x) \\ \rho(t) \end{pmatrix} = \begin{pmatrix} rn(t, x) - d\rho(t)n(t, x) \\ r\rho(t) - d\rho(t)^2 \end{pmatrix} \tag{2.4}$$

The function F defined by :

$$F \begin{pmatrix} n \\ \rho \end{pmatrix} := \begin{pmatrix} rn - d\rho n \\ r\rho - d\rho^2 \end{pmatrix}$$

is $C^1(\mathbb{R}^2)$, so (2.4) has a unique maximal solution on $[0, \infty) \times [0, 1]$ that is thus $(\bar{n}, \bar{\rho})$.

As for any $n \in C^1([0, \infty) \times [0, 1])$ solution of (2.2) , we have that $(n, t \longrightarrow \int_{[0,1]} n(t, x)dx)$ is a solution of (2.4), then we know that there is a unique solution to (2.2) on $[0, \infty) \times [0, 1]$. □

2.2.2 Mutualistic interactions between two populations

We will now focus on the situation with two cell populations interacting with each other. We recall the system previously defined:

$$\begin{cases} \partial_t n_M(t, x) = n_M(t, x) \ [r_M(x) - d_M(x)\rho_M(t) + \rho_E(t)\phi_M(t)] & (t, x) \in [0, \infty) \times [0, 1] \\ \partial_t n_E(t, y) = n_E(t, y) \ [r_E(y) - d_E(y)\rho_E(t) + \rho_M(t)\phi_E(t)] & (t, y) \in [0, \infty) \times [0, 1] \end{cases} \tag{2.1}$$

where for $C, D \in \{M, E\}$:

- The effect of population D on population C at time t is quantified by $\rho_D(t)\phi_C(t)$.

- The total mass of population C at time t is:

$$\rho_C(t) = \int_{[0,1]} n_C(t,z)dz.$$

Our analysis will mainly focus on the ODE version of system (2.1), obtained with the integration of (2.1) over $[0,1]$ and assuming constant birth and death rates:

$$\begin{cases} \rho'_M(t) = \rho_M(t)\ [r_M - d_M\rho_M(t) + \rho_E(t)\phi_M(t)] & (t) \in [0,\infty) \\ \rho'_E(t) = \rho_E(t)\ \ [r_E - d_E\rho_E(t) + \rho_M(t)\phi_E(t)] & (t) \in [0,\infty) \end{cases} \tag{2.3}$$

The two different nature of interactions we will consider are, for $C \in \{M, E\}$:

- $\phi_C(t) = \int_{[0,1]} \psi_C(z) n_C(t,z)dz \quad \forall t \geq 0$
- $\phi_C(t) = \frac{\int_{[0,1]} \psi_C(z) n_C(t,z)dz}{1+\rho_C(t)} \quad \forall t \geq 0$

Constant mutualistic interactions .

In this part we will choose the interaction functions as suggested before, that is for $C \in \{M, E\}$:

$$\phi_C(t) = \int_{[0,1]} \psi_C(z) n_C(t,z)dz.$$

For the sake of simplicity, the parameters $r_M, r_E, d_M, d_E, \psi_M, \psi_E$ will be positive constants. Then system (2.1) rewrites itself:

$$\begin{cases} \partial_t n_M(t,x) = n_M(t,x)\ [r_M - d_M\rho_M(t) + \psi_M\rho_M(t)\rho_E(t)] & (t,x) \in [0,\infty) \times [0,1] \\ \partial_t n_E(t,y) = n_E(t,y)\ [r_E - d_E\rho_E(t) + \psi_E\rho_E(t)\rho_M(t)] & (t,y) \in [0,\infty) \times [0,1] \end{cases} \tag{2.5}$$

By integrating (2.5) over $[0,1]$, one gets the ODE version of the system :

$$\begin{cases} \rho'_M(t) = \rho_M(t)\ [r_M - d_M\rho_M(t) + \psi_M\rho_M(t)\rho_E(t)] & t \in [0,\infty) \\ \rho'_E(t) = \rho_E(t)\ [r_E - d_E\rho_E(t) + \psi_E\rho_E(t)\rho_M(t)] & t \in [0,\infty) \end{cases} \tag{2.6}$$

The objective here is, after proving the existence of a unique maximal solution of (2.6), to figure out the how it shapes up asymptotically. This will give us an idea of the total masses behavior across time, but to complete the study it would be important to work on the partial differential system (2.5).

Let us first show the existence and uniqueness of the solution of (2.6) along with the positivity property of the system.

Proposition 2. For any $(\rho_M^0, \rho_E^0) \in [0, \infty)^2$, (2.6) has a unique maximal solution (ρ_M, ρ_E) that satisfies $(\rho_M(0), \rho_E(0)) = (\rho_M^0, \rho_E^0)$ and that is positive.

Proof. 1. *Existence and uniqueness.*

By Cauchy Lipschitz theorem, existence and uniqueness of a maximal solution comes from $f \in C^1(\mathbb{R}^2)$ where f is defined as:

$$f(\rho_M, \rho_E) = \begin{pmatrix} \rho_M \ [r_M - d_M\rho_M + \psi_M\rho_M\rho_E] \\ \rho_E \ [r_E - d_E\rho_E + \psi_E\rho_E\rho_M] \end{pmatrix}$$

2. *Positivity.* If $\rho_M^0 > 0, \rho_E^0 > 0$.

By contradiction, let T be the minimal time at which $\rho_M(T) = 0$ and $\rho_R(T) > 0$. Then :

$$\begin{cases} \rho_M'(T) = 0 \\ \rho_E'(T) = \rho_E(T) \ [r_E - d_E\rho_E(T)] \end{cases}$$

Then eventually (ρ_M, ρ_E) will reach the steady state $(0, \frac{r_E}{d_E})$. By uniqueness, as the only initial conditions for which this steady state is stable are on the y-axis, we get $(\rho_M(0), \rho_E(0)) = (0, \frac{r_E}{d_E})$ which gives the contradiction.

□

Now we aim to analyse the asymptotic behavior of the solution of system (2.6). We first state the following proposition.

Proposition 3. We denote (ρ_M, ρ_E) a solution of (2.6) and I its maximal interval of existence. Either $|(\rho_M(t), \rho_E(t))| \to \infty$ as $t \to \partial I_+$, or else $(\rho_M(t), \rho_E(t))$ converges to a stable steady point as $t \to \partial I_+$.

Proof. As (2.6) is a two dimensional cooperative 2 by 2 system, according to an application of Poincarré-Bendixon theorem given in [11], the result is true. □

We must perform a stability analysis of the steady states of (2.6). Our objective is to get a general idea of the asymptotics and some computations are complicated so we will for clarity sketch the different phase portraits for various cases based on the values of the parameters, made with Maple. The colored curves represent random trajectories and the green and red dots are the equilibria. Afterwards we will investigate the nature of the maximal interval of existence.

The steady points of this ODE system are:

$$(0, 0), (0, \frac{r_E}{d_E}), (\frac{r_M}{d_M}, 0)$$

and other possible ones given by $(\bar{\rho_M}, \bar{\rho_E})$ the solutions of:

$$\begin{cases} -\bar{\rho_M}^2 \psi_M d_M + \bar{\rho_M}(d_M d_E - \psi_E r_E + r_M \psi_M) - r_M d_E = 0 \\ \bar{\rho_E}(d_E - \psi_M \bar{\rho_M}) = r_E \end{cases} \tag{2.7}$$

The Jacobian matrix of the system (2.6) is given by:

$$J(\rho_M, \rho_E) = \begin{pmatrix} r_M - 2d_M\rho_M + 2\psi_E\rho_M\rho_E & \rho_M^2\psi_E \\ \rho_E^2\psi_M & r_E - 2d_E\rho_E + 2\psi_M\rho_E\rho_M \end{pmatrix}$$

By evaluating the Jacobian matrix at the equilibria $(0,0)$, $(0, \frac{r_E}{d_E})$ and $(\frac{r_M}{d_M}, 0)$, we get that $(0,0)$ is an unstable repelling node and both $(0, \frac{r_E}{d_E})$ and $(\frac{r_M}{d_M}, 0)$ are unstable saddle points.

We wish to examine whether there are other steady points and if they are stable or not. The existence of solutions for system (2.7) is given by the sign of:

$$\Delta = (d_M d_E - \psi_E r_E + r_M \psi_M)^2 - 4 r_M d_E \psi_M d_M.$$

We study the three possible cases:

- $\Delta < 0$.

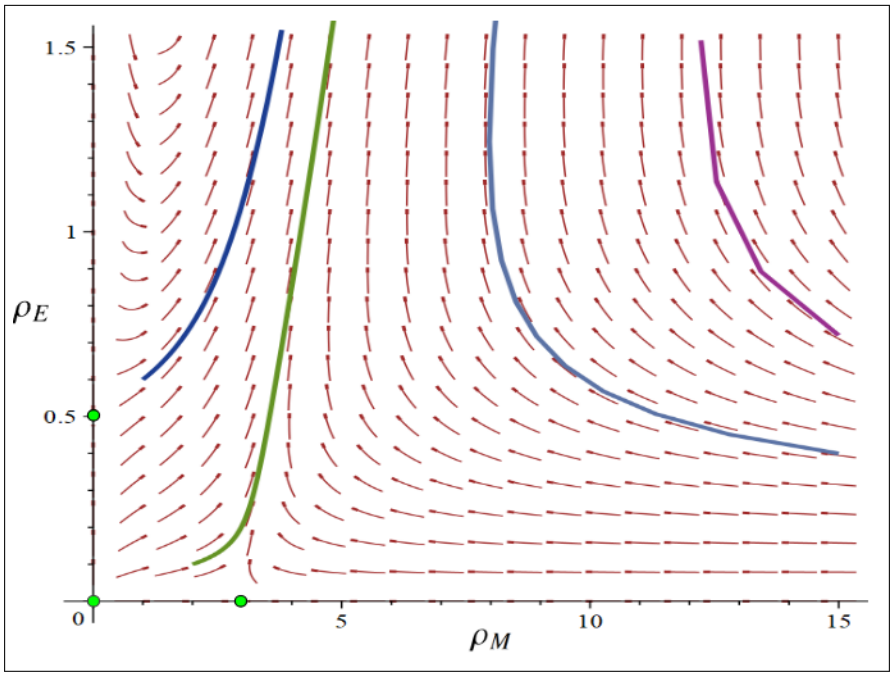

Figure 2.1: Phase portrait for $\Delta < 0$
$r_M = 3$; $r_E = 1$; $d_M = 1$; $d_E = 2$; $\psi_M = 0.5$; $\psi_E = 1$

Then there is no other steady point and none of the steady points are stable neither asymptotically stable. So according to **Proposition 3** $|(\rho_M(t), \rho_E(t))| \to \infty$ as $t \to \partial I_+$; the solution explodes.

Example 1. We will here focus on the simple case where:

$$\begin{cases} r := r_M = r_E \\ d := d_M = d_E \\ \psi := \psi_M = \psi_E \\ \rho_0 := \rho_M(0) = \rho_E(0) \end{cases}$$

Proposition 4. In this particular case, $\rho_M(t) = \rho_E(t)$ for all $t \in [0, \infty]$.

Proof. The system writes:

$$\begin{cases} \rho'_M(t) = \rho_M(t)\ [r - d\rho_M(t) + \psi\rho_M(t)\rho_E(t)] & t \in [0, \infty) \\ \rho'_E(t) = \rho_E(t)\ [r - d\rho_E(t) + \psi\rho_E(t)\rho_M(t)] & t \in [0, \infty) \\ \rho_M(0) = \rho_E(0) \end{cases} \tag{2.8}$$

The result is straightforward from **Proposition 2** as (ρ, ρ) is a solution of (2.8) where ρ satisfies:

$$\begin{cases} \rho'(t) = \rho(t)\ [r - d\rho(t) + \psi\rho(t)^2], \text{ for } t \in [0, \infty) \\ \rho(0) = \rho_0 \end{cases} \tag{2.9}$$

□

We have thus reduced to system (2.9). We assume moreover that $d^2 < 4.r.\psi$ in order to ensure $\Delta < 0$.

We notice:

$$\frac{1}{(r - d\rho + \psi\rho^2)\rho} = \frac{2d - 2\psi\rho}{2r(r - d\rho + \psi\rho^2)} + \frac{1}{r\rho} = \frac{d - 2\psi\rho}{2r(r - d\rho + \psi\rho^2)} + \frac{d}{2r\psi}\frac{1}{(\rho - \frac{d}{2\psi})^2 + \frac{4r\psi - d^2}{4\psi^2}} + \frac{1}{r\rho}$$

Integrating yields:

$$C + \tau = -\frac{1}{2r}\ln|r - d\rho + \psi\rho^2| + \frac{2d\psi}{r(4r\psi - d^2)}\arctan\left(\frac{2\psi\rho - d}{\sqrt{4r\psi - d^2}}\right) + \frac{1}{r}\ln|\rho|$$

where $\rho = \rho(\tau)$ and $C = \frac{1}{r}\ln\frac{|\rho_0|}{\sqrt{r - d\rho_0 + \psi\rho_0^2}} + \frac{2d\psi}{r(4r\psi - d^2)}\arctan\left(\frac{2\psi\rho_0 - d}{\sqrt{4r\psi - d^2}}\right)$ is the integration constant.

Equivalently:

$$C + \tau = -\frac{1}{r}\ln\frac{|\rho|}{\sqrt{r - d\rho + \psi\rho^2}} + \frac{2d\psi}{r(4r\psi - d^2)}\arctan\left(\frac{2\psi\rho - d}{\sqrt{4r\psi - d^2}}\right).$$

Under the hypothesis that ρ explodes, one gets:

$$\tau^* + C = -\frac{1}{r}\ln\frac{1}{\sqrt{\psi}} + \frac{2d\psi}{r(4r\psi - d^2)}.\frac{\pi}{2}.$$

Consequently in this particular setting, the blow up happens in finite time τ^* computed above.

Back into the more general case, a similar argumentation provides a lower bound for the time of explosion, as done below.

Let $u = \sqrt{\rho_M \rho_E}$. Then :

$$u'(t) = \frac{\rho'_M(t)\rho_E(t) + \rho_M(t)\rho'_E(t)}{2\sqrt{\rho_M(t)\rho_E(t)}}$$

$$= \frac{u(t)}{2}[r_M + r_E - d_M\rho_M(t) - d_E\rho_E(t) + (\psi_M + \psi_E)u(t)^2] \leq \frac{u(t)}{2}[r_M + r_E - 2u(t)\sqrt{d_M d_E} + (\psi_M + \psi_E)u(t)^2]$$

Let us have a look at the polynomial: $\mathcal{P}(u) = r_M + r_E - 2u\sqrt{d_M d_E} + (\psi_M + \psi_E)u^2$.

$$\Delta_u = 4d_M d_E - 4(\psi_M + \psi_E)(r_M + r_E)$$

$$= 4(d_M d_E - \psi_M r_M - \psi_M r_E - \psi_E r_M - \psi_E r_E)$$

$$= 4(d_M d_E - (\sqrt{r_M \psi_E} + \sqrt{r_E \psi_M})^2 - (\sqrt{r_M \psi_M} - \sqrt{r_E \psi_E})^2)$$

$$\leq 4(d_M d_E - (\sqrt{r_M \psi_E} + \sqrt{r_E \psi_M})^2 < 0$$

Because $\Delta < 0$.

The computations done in Example 1 give in this more general setting that the time of blow up τ^* satisfies :

$$\frac{\Psi D \pi}{R(4\Psi R - D^2)} \leq \tau^* + C$$

where: $C = \frac{1}{R} \ln \frac{u_0^2}{R - D u_0 + \Psi u_0^2} + \frac{4D\Psi}{R(4R\Psi - D^2)} \arctan(\frac{2\Psi u_0 - D}{\sqrt{4R\Psi - D^2}})$ is the integration constant and:

$$\begin{cases} R := r_M + r_E \\ D := 2\sqrt{d_M d_E} \\ \Psi := \psi_M + \psi_E \end{cases}$$

- $\Delta = 0$.

  In that case, there is a forth steady point :

$$(\bar{\rho_M}, \bar{\rho_E}) = (\sqrt{\frac{r_M d_E}{\psi_M d_M}}, \sqrt{\frac{r_E d_M}{\psi_E d_E}}).$$

  Then :

$$|J(\bar{\rho_M}, \bar{\rho_E}) - \lambda| = \begin{bmatrix} -r_M - \lambda & \frac{\psi_E r_M d_E}{\psi_M d_M} \\ \frac{\psi_M r_E d_M}{\psi_E d_E} & -r_E - \lambda \end{bmatrix}$$

$$= (r_M + \lambda)(r_E + \lambda) - r_M r_E = \lambda(\lambda + r_M + r_E).$$

As the two eigenvalues 0 and $-(r_M + r_E)$ are non positive and not both negative, it would require further theoretical investigation to determinate if this equilibrium $(\bar{\rho_M}, \bar{\rho_E})$ is asymptotically stable, which will not be done here.

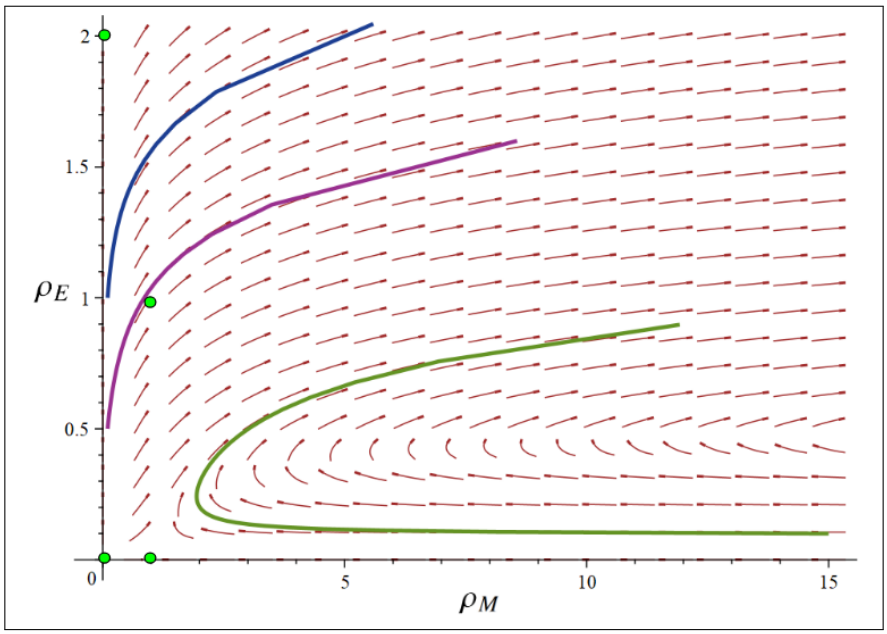

Figure 2.2: Phase portrait for $\Delta = 0$
$r_M = 4$; $r_E = 2$; $d_M = 4$; $d_E = 1$; $\psi_M = 1$; $\psi_E = 8$

However we can conjecture from the phase portrait in Figure 2.2 that some initial conditions lead to explosion to $+\infty$.

- $\Delta > 0$. In that case, there exists two more steady points than in the case $\Delta < 0$, given by:

$$(\bar{\rho_{M,1}} = \frac{d_M d_E - \psi_E r_E + r_M \psi_M + \sqrt{\Delta}}{2\psi_M d_M}, \quad \bar{\rho_{E,1}} = \frac{2 r_E d_M}{d_M d_E + \psi_E r_E - r_M \psi_M - \sqrt{\Delta}})$$

$$(\bar{\rho_{M,2}} = \frac{d_M d_E - \psi_E r_E + r_M \psi_M - \sqrt{\Delta}}{2\psi_M d_M}, \quad \bar{\rho_{E,2}} = \frac{2 r_E d_M}{d_M d_E + \psi_E r_E - r_M \psi_M + \sqrt{\Delta}})$$

The stability analysis computations are here complicated so we will focus on a particular example and with the help of the phase portrait in Figure 2.3 we will get a good understanding of the dynamics.

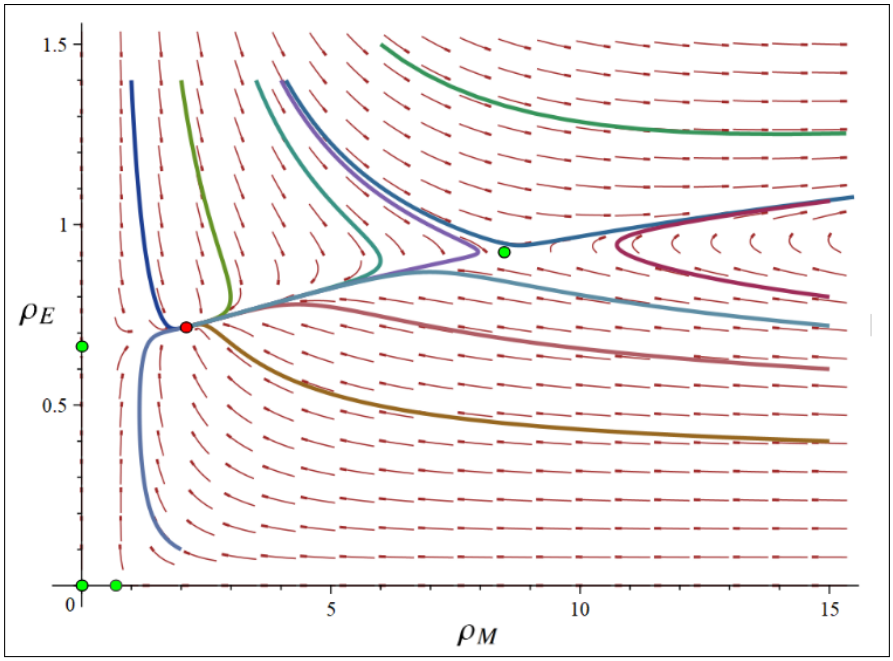

Figure 2.3: Phase portrait for $\Delta > 0$
$r_M = 0.6$; $r_E = 2$; $d_M = 1$; $d_E = 3$; $\psi_M = 1$; $\psi_E = 0.1$

Example 2. We look at the simple case where:

$$\begin{cases} r := r_M = r_E \\ d := d_M = d_E \\ \psi := \psi_M = \psi_E \\ \rho_0 := \rho_M(0) = \rho_E(0) \end{cases}$$

But this time we assume that $d^2 > 4.r.\psi$ in order to ensure $\Delta > 0$. System (2.7) boils down to :

$$\begin{cases} -\bar{\rho_M}^2\psi + \bar{\rho_M}d - r = 0 \\ \bar{\rho} := \bar{\rho_E} = \bar{\rho_M} \end{cases}$$

Then the Jacobian writes:

$$|J(\bar{\rho}) - \lambda| = \begin{bmatrix} -r-\lambda & \bar{\rho}^2\psi \\ \bar{\rho}^2\psi & -r-\lambda \end{bmatrix} = \lambda^2 + 2\lambda r + r^2 - \psi^2\bar{\rho}^4$$

The solutions are given by: $\lambda_\pm = -r \pm \psi\bar{\rho}^2$.

So we already know that $\lambda_- < 0$ for both equilibria $(\rho_{\bar{M},1}, \rho_{\bar{E},1})$ and $(\rho_{\bar{M},2}, \rho_{\bar{E},2})$.

Concerning λ_+, the two possible solutions $\bar{\rho_1}$, $\bar{\rho_2}$ are given by:

$$\bar{\rho_{1,2}} = \frac{d \pm \sqrt{d^2 - 4r\psi}}{2\psi} \geq 0$$

So:

$$\begin{cases} \lambda_{+,1} = -r + \psi \bar{\rho_1}^2 = -2r + d\bar{\rho_1} = -2r + \frac{d}{2\psi}(d - \sqrt{d^2 - 4r\psi}) \\ \lambda_{+,2} = -r + \psi \bar{\rho_2}^2 = -2r + d\bar{\rho_2} = -2r + \frac{d}{2\psi}(d + \sqrt{d^2 - 4r\psi}) \end{cases}$$

Quick calculations give $\lambda_{+,2} > 0$ and $\lambda_{+,1} < 0$ thanks to the hypothesis $d^2 > 4r\psi$.

Gathering up : $(\bar{\rho_M}_{,2}, \bar{\rho_E}_{,2})$ is an unstable saddle point and $(\bar{\rho_M}_{,1}, \bar{\rho_E}_{,1})$ (in red on Figure 2.3) is locally asymptotically stable.

For any value of $\Delta \in \mathbb{R}$, it is clear from the phase portraits that some initial conditions lead to the explosion to $+\infty$ of the solutions. Next we aim to investigate whether this blow up occurs in finite or infinite time.

Proposition 5. For system (2.6), the solution (ρ_M, ρ_E) explodes to $+\infty$ in finite time if and only if both ρ_M and ρ_E explode.

Proof. Assume $\lim_t \rho_M(t) = +\infty$. Then we distinguish the different cases:

- If $\lim_t \rho_E(t) = +\infty$. Then asymptotically, from (2.6) we get :

$$\begin{cases} \rho'_M(t) \approx \psi_M \rho_M(t)^2 \rho_E(t) \\ \rho'_E(t) \approx \psi_E \rho_E(t)^2 \rho_M(t) \end{cases}$$

So asymptotically:

$$\frac{\partial \rho_M}{\partial \rho_E}(\rho_E) = \frac{\frac{\partial \rho_M}{\partial t}}{\frac{\partial \rho_E}{\partial t}} \approx \frac{\psi_M \rho_M(\rho_E)}{\psi_E \rho_E}.$$

Implying that asymptotically :

$$\rho_M(\rho_E) \approx \rho_E^{\frac{\psi_M}{\psi_E}}.$$

Then asymptotically:

$$\rho'_E(t) \approx \psi_E \rho_E(t)^\alpha$$

where $\alpha = 2 + \frac{\psi_M}{\psi_E} < 1$.

The solution of this ODE satisfies:

$$\rho_E(t)^{1-\alpha} = (1-\alpha)t + \rho_E(0)^{1-\alpha}$$

which explodes in finite time. This concludes one implication. For the other one:

- If $\lim_t \rho_E(t) = 0$ (up to a sub-sequence). Then asymptotically, from (2.6) we get :

$$\begin{cases} \rho'_M(t) \approx \rho_M(t)(r_M - d_M\rho_M(t)) \\ \rho'_E(t) \approx \rho_E(t)(r_E + \psi_E\rho_M(t)\rho_E(t)) \end{cases}$$

  So ρ_M does not explode in finite time, see section 2.2.1.

- If $\lim_t \rho_E(t) = C \neq 0$ (up to a sub-sequence). Then (ρ_M, ρ_E) must converge to an equilibrium, which contradicts our hypothesis : $\lim_t \rho_M(t) = +\infty$.

□

This proposition allows us to conclude that for any parameter configuration, there exists initial conditions for which the solution of the system (2.6) blows up in finite time. In suffices to choose ρ_M^0 and ρ_E^0 big enough so that near 0:

$$\begin{cases} \rho'_M(t) \approx \psi_M\rho_M(t)^2\rho_E(t) \\ \rho'_E(t) \approx \psi_E\rho_E(t)^2\rho_M(t) \end{cases}$$

However this is not a biological observable reality so our model needs to be refine. To prevent finite time blow-up and thereby enhance the model's ability to replicate biological observations, we will modify the interaction dynamics described by the functions ϕ_C.

Saturated mutualistic interactions .

In this section we suggest saturated interactions, that is we take functions ϕ_C, for $C = M, E$ of the form :

$$\phi_C(t) = \frac{\psi_C\rho_C(t)}{1 + \rho_C(t)} \quad \text{with } \psi_C > 0.$$

Then for any $t > 0$, $\phi_C(t) \leq \psi_C$ ensuring an upper bound for the interactions.

System (2.1) becomes in this case:

$$\begin{cases} \partial_t n_M(t,x) = n_M(t,x)\ [r_M(x) - d_M(x)\rho_M(t) + \rho_E(t)\psi_M \frac{\rho_M(t)}{1+\rho_M(t)}] & (t,x) \in [0,\infty) \times [0,1] \\ \partial_t n_E(t,y) = n_E(t,y)\ [r_E(y) - d_E(y)\rho_E(t) + \rho_M(t)\psi_E \frac{\rho_E(t)}{1+\rho_E(t)}] & (t,y) \in [0,\infty) \times [0,1] \end{cases} \tag{2.10}$$

And its ODE version when taking constant coefficients r_M, r_E, d_M, d_E:

$$\begin{cases} \rho'_M(t) = \rho_M(t)\ [r_M - d_M\rho_M(t) + \rho_E(t)\psi_M \frac{\rho_M(t)}{1+\rho_M(t)}] & t \in [0,\infty) \\ \rho'_E(t) = \rho_E(t)\ [r_E - d_E\rho_E(t) + \rho_M(t)\psi_E \frac{\rho_E(t)}{1+\rho_E(t)}] & t \in [0,\infty) \end{cases} \tag{2.11}$$

The modeling hypothesis here is that the message going from population M (resp. E) to population E (resp. M) becomes saturated when the density of population E (resp. M) grows excessively.

The steady states of this ODE system are:

$$(0,0), (0, \frac{r_E}{d_E}), (\frac{r_M}{d_M}, 0)$$

and other possible ones given by $(\bar{\rho_M}, \bar{\rho_E})$ the solutions of:

$$\begin{cases} \bar{\rho_M}^2 d_M + \bar{\rho_M}(d_M - r_M - \psi_M \bar{\rho_E}) + r_M = 0 \\ \bar{\rho_E}^2 d_E + \bar{\rho_E}(d_E - r_E - \psi_E \bar{\rho_M}) + r_E = 0. \end{cases} \tag{2.12}$$

A complete stability analysis should be done in this case but in this report we will restrict ourselves to the numerical analysis of the model with saturated interactions.

2.3 Numerical analysis

In this section we will detail the numerical method used to resolve the system and then display the numerical results obtained with Python. While waiting for biological clarifications we computed codes that could easily be reused for similar PDE models. The last subsection is dedicated to a small introduction to numerical optimal control.

2.3.1 Introduction to the numerical model

For this numerical analysis, under Franck Alvarez's guidance, we considered two-dimensional phenotypes : $x := (x_1, x_2)$ for macrophages and $y := (y_1, y_2)$ for epithelial cells, enabling the model to gain in complexity in the case where the biological concerns require to add another phenotypic variable.

Let T_f be the final finite time of the simulations. The general model is then :

$$\begin{cases} \partial_t n_M(t, x_1, x_2) = n_M(t, x_1, x_2) \ [r_M(x_1, x_2) - d_M(x_1, x_2)\rho_M(t) + \rho_E(t)\phi_M(t)] & (t, x_1, x_2) \in [0, T_f] \times [0,1]^2 \\ \partial_t n_E(t, y_1, y_2) = n_E(t, y_1, y_2) \ [r_E(y_1, y_2) - d_E(y_1, y_2)\rho_E(t) + \rho_M(t)\phi_E(t)] & (t, y_1, y_2) \in [0, T_f] \times [0,1]^2 \end{cases} \tag{2.13}$$

To discretize (2.13) one typical way of proceeding (as in [9]) is to use the finite volume method:

Let $N \in \mathbb{N}$ be the number of nodes in each space of phenotypes $[0, 1]$. We define the following control volumes:

$$C^{ij} = [\frac{i}{N}, \frac{i+1}{N}] \times [\frac{j}{N}, \frac{j+1}{N}] \ \text{ for } i, j = 0, ..., N-1 \text{ s.t } \cup C^{ij} = [0,1]^2$$

For $z \in \{x, y\}$ and $i, j \in \{0, .., N-1\}$, we denote by (z_1^i, z_2^j) the center of cell C^{ij}. The area of every square C^{ij} is $\frac{1}{N^2}$.

For $C \in \{M, E\}$ and $z \in \{x, y\}$ we will proceed to the following approximation coming from the finite volume method:

$$n_C(t, z_1^i, z_2^j) \approx n_C^{ij}(t) := N^2 \int_{C^{ij}} n_C(t, z_1, z_2) dz \quad \forall i, j \in \{0, ...N-1\}.$$

We get rid of the double indexation $\{ij\}$ by introducing $l := N(i-1) + j, \quad l \in 1, ..., N^2$.

Then:

$$n_C(t, z^l) \approx n_C^l(t) := N^2 \int_{C^l} n_C(t, z^l) dz \quad \forall l \in \{0, ...N^2\}$$

where the above new notations z^l, n_C^l and C^l follow naturally. Thereafter we get:

$$\rho_C(t) = \int_{[0,1]^2} n_C(t, z) dz = \int_{\cup C^l} n_C(t, z) dz = \sum_l \int_{C^l} n_C(t, z) dz \approx \frac{1}{N^2} \sum_l n_C^l(t)$$

.

and similarly for any regular function $f : z = (z_1, z_2) \longrightarrow f(z_1, z_2)$:

$$\int_{C^l} n_C(t, z) f(z) dz \approx \frac{1}{N^2} n_C^l(t) f^l$$

.

where : $f^l := f(z^l)$ for any $l \in \{0, ..., N^2\}$.

By integrating system (2.13) on C^l for a given $l \in 0, ..., N^2$ and multiplying by N^2 we get an ODE system:

$$\begin{cases} n_M^{l\prime}(t) = n_M^l(t) \ [r_M^l - \frac{d_M^l}{N^2} \sum_l n_M^l(t) + \frac{1}{N^2} \sum_l n_E^l(t) \phi_M(t)] & t \in [0, T_f], l \in \{0, ..N^2\} \\ n_E^{l\prime}(t) = n_E^l(t) \ [r_E^l - \frac{d_E^l}{N^2} \sum_l n_E^l(t) + \frac{1}{N^2} \sum_l n_M^l(t) \phi_E(t)] & t \in [0, T_f], l \in \{0, ..N^2\} \end{cases}$$

Where we assumed some regularity of the solution to differentiate under the integral sign.

We use the implicit Euler scheme to discretize this system over time. Let T be the number of temporal nodes in $[0, T_f]$ and $\Delta t = \frac{T_f}{T}$ and $t_k = k\Delta t$ for $k \in \{0, .., T\}$.

Let $C \in \{M, E\}$, $l \in \{0, ..., N^2\}$ and $k \in \{0, ..., T\}$. We denote respectively $n_{C,k}^l$ and $\phi_{C,k}$ the approximations of $n_C^l(t_k)$ and $\phi_C(t_k)$. We have:

$$\begin{cases} n_{M,k+1}^l [1 - r_M^l \Delta t + \frac{d_M^l \Delta t}{N^2} \sum n_{M,k+1}^l - \frac{\Delta t}{N^2} \sum n_{E,k+1}^l \phi_{M,k+1}] = n_{M,k}^l \\ n_{E,k+1}^l [1 - r_E^l \Delta t + \frac{d_E^l \Delta t}{N^2} \sum n_{E,k+1}^l - \frac{\Delta t}{N^2} \sum n_{M,k+1}^l \phi_{E,k+1}] = n_{E,k}^l \end{cases} \tag{2.14}$$

The numerical computations are heavy so the codes directly derived from (2.14) are unusable. Therefore we will use a technique used by the authors of [9] to optimize the scheme. It consists of handling large sparse matrices in order to gain time on computations.

We introduce $I_{C,k} = \frac{1}{N^2}\sum_l n^l_{C,k}$ and the generalized variable $\underline{n}_{C,k} = (n_{C,k}, I_{C,k})$ where $n_{C,k} = (n^l_{C,k})_{l=0,...,N^2}$. Then summing (2.14) over l and dividing by N^2, for $D \in \{M, E\}$, $D \neq C$:

$$I_{C,k} = I_{C,k+1} - \frac{\Delta t}{N^2}\sum r^l_C n^l_{C,k+1} + \frac{I_{C,k+1}\Delta t}{N^2}\sum d^l_C n^l_{C,k+1} - \Delta t I_{D,k+1} I_{C,k+1}\phi_{C,k+1}$$

So the generalized scheme is:

$$\begin{cases} n^l_{C,k} = n^l_{C,k+1}[1 - r^l_C\Delta t + d^l_C\Delta t I_{C,k+1} - \Delta t I_{D,k+1}\phi_{C,k+1}] & l = 0, ..., N^2 \\ I_{C,k} = I_{C,k+1} - \frac{\Delta t}{N^2}\sum r^l_C n^l_{C,k+1} + \frac{I_{C,k+1}\Delta t}{N^2}\sum d^l_C n^l_{C,k+1} - \Delta t I_{D,k+1} I_{C,k+1}\phi_{C,k+1} \end{cases}$$

We can gather the generalized systems on M and E with a vector equality:

$$Mat(\underline{n}_{k+1})\cdot\underline{n}_{k+1} - \underline{n}_k = 0 \tag{2.15}$$

where $\underline{n}_k = (\underline{n}_{M,k}, \underline{n}_{E,k})$ and $Mat(\underline{n}_{k+1})$ is a square matrix of size $2N^2 + 2$. We will not here give the specific calculations.

Then at each time k step we use the Newton-Raphson method to solve (2.15).

The choice of initial conditions we have made is similar to the one in [9] of the form :

$$n_{C,0}(z_1, z_2) = \mathbb{1}_{\{g_C(z_1,z_2)<1\}} e^{-\frac{1}{1-g_C(z_1,z_2)}}$$

for $C \in \{M, E\}$ where :

· $g_M : (z_1, z_2) \longrightarrow \frac{(z_1-0.25)^2+(z_2-0.25)^2}{(0.25)^2}$

· $g_E : (z_1, z_2) \longrightarrow \frac{(z_1-0.75)^2+(z_2-0.75)^2}{(0.25)^2}$

This represents an initial situation where the phenotypes are concentrated around set phenotypes: $(0.25, 0.25)$ for the macrophage population and $(0.75, 0.75)$ for the epithelial one, as illustrated on Figure 2.4. This suggestion seems consistent with the biological observations, as the macrophages are suspected to present a M1 phenotype at the beginning of the carcinogenesis that will undergo a M2 switch. For the epithelial cells it corresponds to the hypothesis that epithelial cells have a high differentiation potential in early stages which would need to be corroborated biologically in the context of oral cancers.

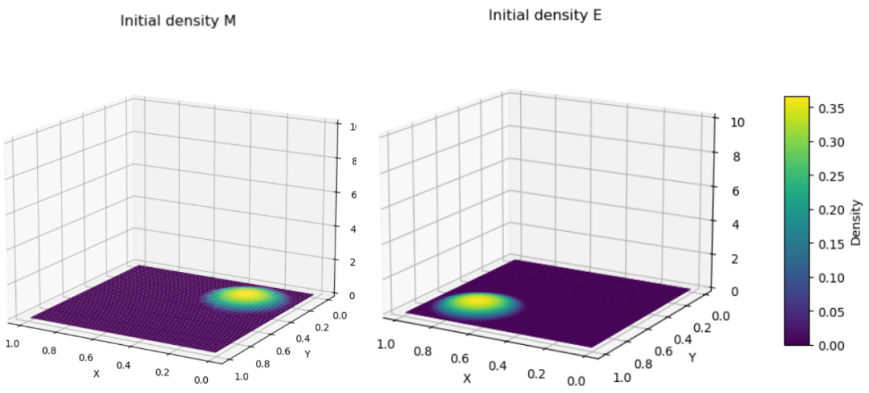

Figure 2.4: Initial densities

2.3.2 Constant mutualistic interactions

In this subsection we illustrate the solutions of the two-dimensional model when the interactions are mutualistic and constant. The numerical scheme reduces to:

$$\begin{cases} n^l_{C,k} = n^l_{C,k+1}[1 - r^l_C \Delta t + d^l_C \Delta t I_{C,k+1} - \Delta t I_{D,k+1} \psi_C I_{C,k+1}] & l = 0, ..., N^2 \\ I_{C,k} = I_{C,k+1}(1 + \frac{\Delta t}{N^2} \sum d^l_C n^l_{C,k+1} - \Delta t I_{D,k+1} I_{C,k+1} \psi_C) - \frac{\Delta t}{N^2} \sum r^l_C n^l_{C,k+1} \end{cases}$$

We illustrate in Figure 2.5 the final densities ($T_f = 40$) of the two populations having constant mutualistic interactions. As choice of parameters and in absence of accurate biological knowledge we took $r := r_M = r_E$, $d := d_M = d_E$ and $\psi := \psi_M = \psi_E$ constant equal to respectively 0.6, $2\sqrt{r}$ and 1.

These values imply $\Delta = 0$ in which case there is a stable equilibrium $(\sqrt{0.6}, \sqrt{0.6})$ as seen before.

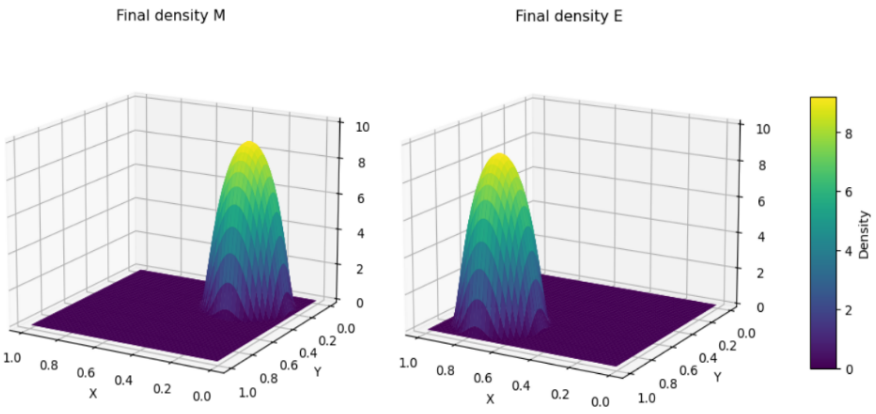

Figure 2.5: Final densities with constant interactions

We observe that both densities have concentrated around the fixed initial phenotypes, and both total masses represented in Figure 2.6 increase over time. We also conjecture the convergence of the total masses (ρ_M, ρ_E) towards the equilibrium $(\sqrt{0.6}, \sqrt{0.6})$.

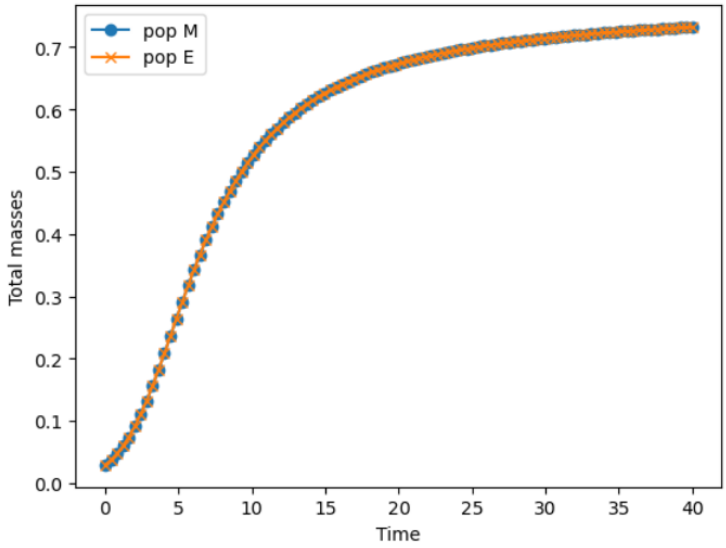

Figure 2.6: Evolution of total masses with time (constant interactions)

When choosing other parameters values we observe a blow up in finite time characterized by negative numerical solutions that is not interesting to illustrate here but that allowed us to find out that the model was not satisfactory.

We also plot on Figure 2.7 the case where there is no interactions between the two populations, corresponding to the situation of two uncoupled single integro-differential equations.

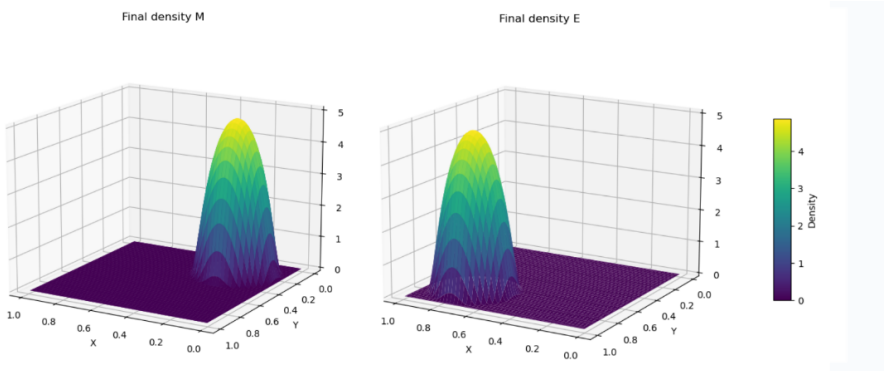

Figure 2.7: Final densities with no interaction

We observe that both densities have concentrated around the fixed initial phenotypes but as we could have expect the concentrations are less marked than in the mutualistic interactions case.

2.3.3 Saturated mutualistic interactions

To avoid the blowing up of solutions we here simulate the solutions of the case with saturated mutualistic interactions. The scheme now writes:

$$\begin{cases} n^l_{C,k} = n^l_{C,k+1}[1 - r^l_C \Delta t + d^l_C \Delta t I_{C,k+1} - \Delta t I_{D,k+1} \psi_C I_{C,k+1} \frac{1}{1+I_{C,k+1}}] & l = 0, ..., N^2 \\ I^{C,k} = I_{C,k+1}(1 + \frac{\Delta t}{N^2} \sum d^l_C n^l_{C,k+1} - \Delta t I_{D,k+1} I_{C,k+1} \psi_C \frac{1}{1+I_{C,k+1}}) - \frac{\Delta t}{N^2} \sum r^l_C n^l_{C,k+1} \end{cases}$$

In Figure 2.8 we illustrate both final time densities in this case with the same choice of parameters as before.

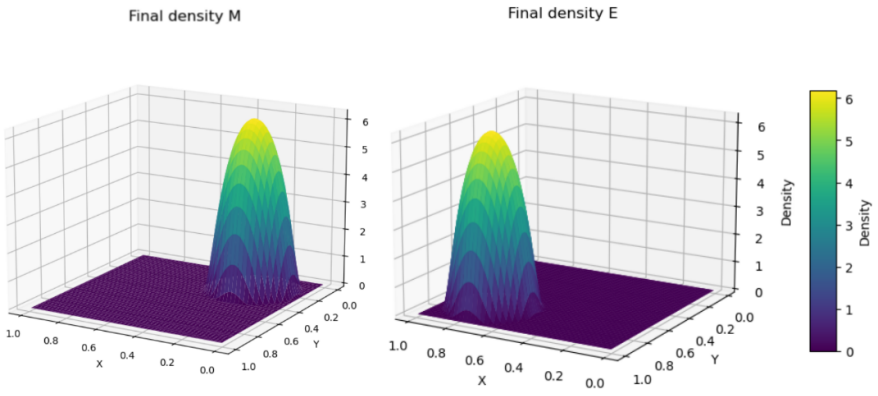

Figure 2.8: Final densities with saturated interactions

We observe the same mechanism of concentration around the initial set phenotypes. Moreover when implementing the code for random choices of parameters we observe this time no more finite time blow up.

When plotting the code for $r = 0.8$, $d = 0.8$ and $\psi = 1$ we observe non-monotonous total masses as in Figure 2.9.

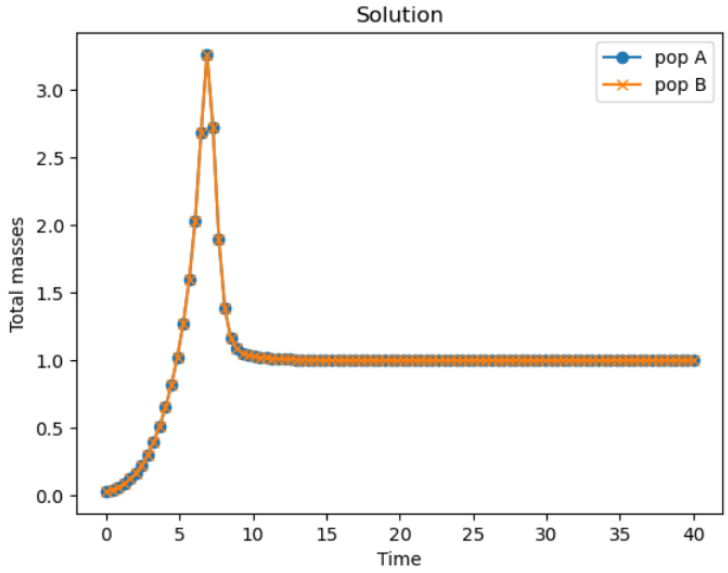

Figure 2.9: Evolution of total masses with time (saturated interactions)

It appears that above a certain threshold the saturation constrains the total masses to decrease. This would be an interesting phenomenon to study theoretically.

2.3.4 Numerical optimal therapeutic control

Optimal control is a branch of applied mathematics that has been widely used for several years, and that seeks to optimize the solution of a differential system under given constraints. Recently it has been used in clinical contexts such as optimal therapeutic control in cancer. In our case, a typical quantity we want to minimize would be the total mass of the cancerous epithelial population.

In this report we achieved a initiation to numerical optimal therapeutic control with the help of AMPL which is a very useful tool that solves numerically optimal control problems. The long term intention is to compare the results obtained with therapeutic biological data on immunotherapies that Jean-Phillipe Foy and his collaborators plan to produce.

Here, and following this report's approach we implement a generic optimization problem. The controlled dynamical system we consider is:

$$\begin{cases} \partial_t n_M(t,x) = \frac{n_M(t,x)}{1+\nu_M v(t)} \left(\alpha w(t) r_M - d_M \rho_M(t) - \mu_M u(t) + \rho_M(t)\rho_E(t)\right) & (t,x) \in [0,T_f] \times [0,1] \\ \partial_t n_E(t,y) = \frac{n_E(t,y)}{1+\nu_E v(t)} \left(r_E - d_E \rho_E(t) - \mu_E u(t) + \rho_E(t)\rho_M(t)\right) & (t,y) \in [0,T_f] \times [0,1] \\ n_C(0,x) = n_C^0(x) \geq 0 & x \in [0,1] \quad C \in \{M,E\} \end{cases} \tag{2.16}$$

It represents the constant mutualistic interactions case with one-dimensional phenotypes and 3 control terms:

- $u \geq 0$, scaled by $\mu \geq 0$: reproduces the action of a cytotoxic drug, killing proliferating cells
- $v \geq 0$, scaled by $\nu \geq 0$: reproduces the action of a cytostatic drug, inhibiting proliferation
- $w \geq 0$, scaled by $\alpha \geq 0$: reproduces the action of an immunotherapy, boosting the macrophage growth

And we want to minimize $\rho_A(T_f)$ under the constraints, for $t \in [0,T_f]$:

$$\begin{cases} 0 < \rho_M(t) < 2\rho_M(0) \\ 0 < \rho_E(t) < 2\rho_E(0) \\ \int_{[0,T]} u(t)dt \leq u_1 \text{ and } u(t) \leq u_\infty \\ \int_{[0,T]} v(t)dt \leq v_1 \text{ and } v(t) \leq v_\infty \\ \int_{[0,T]} w(t)dt \leq w_1 \text{ and } w(t) \leq w_\infty \end{cases}$$

As in [12] we bounded the $\mathcal{L}^1$ and $\mathcal{L}^\infty$ norms of the controls which seams reasonable as they represent drug doses. We also imposed constraints to keep both total masses bounded over time.

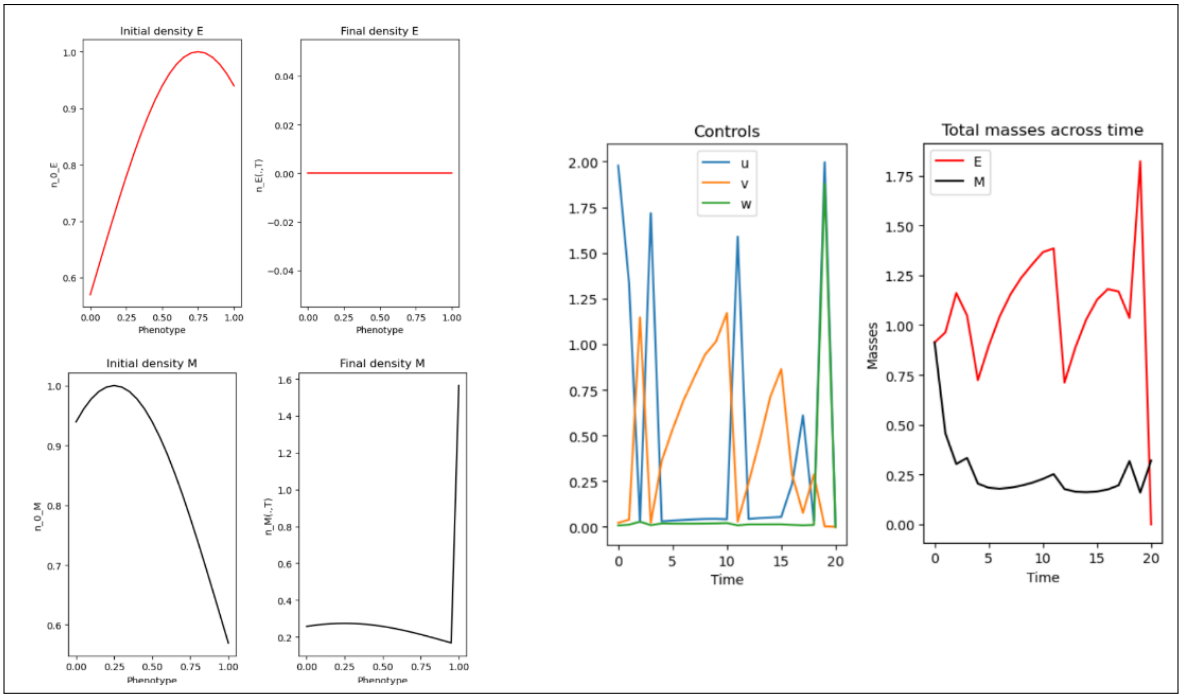

Figure 2.10: Numerical simulations of optimal control problem (2.16)

An optimal solution was found by AMPL and the numerical results are illustrated in Figure 2.10.

We chose initial densities similarly as before but here with one dimensional phenotypes. We observe that at the final time the epithelial population has reduced to 0 and the macrophage phenotypes has gathered around 1. We plotted the optimal controls as functions of time and the evolution of the total masses under these controls.

These results need further investigation as well as theoretical knowledge to be better understood.

Perspectives

As explained in introduction the main aspiration of this study is to lay the groundwork for the coming PhD for which the subject was designed during the internship in collaboration with Jean Clairambault, Emmanuel Trélat and Jean-Phillipe Foy.

Therefore a significant part of the work was to establish the exchanges between medicine, mathematics and computing : what biological concerns are relevant to study through modeling and how to do so? Our answer to that question is not yet complete and needs to be further developed, notably through more biological data that is to come. In particular to have a better understanding of the pro or anti tumorigenic role of macrophages our models need to be refined : the choice of the birth rate $r(.)$, the death rate $d(.)$ and the nature of interactions $\phi(.)$ are to be specified.

The other part of the work was to study generic models both numerically and theoretically in order to have a better view on the behavior of the solutions. We saw that the case of constant mutualistic interactions leads to a blow up of the solutions in finite time which is not relevant biologically. We then enhanced this first model by adding a saturation to the interactions which brought more interesting results. There are still many ways to explore on this subject and this study raised many discussions.

Bibliography

[1] Paré et al. Cancers de la cavité buccale : facteurs de risque et prise en charge. *La Presse Médicale*, 46(3):320–330, 2017.

[2] Leemans et al. The molecular landscape of head and neck cancer. *Nature Reviews Cancer*, 18(5):269–282, 2018.

[3] Foy et al. Early changes in the immune microenvironment of oral potentially malignant disorders reveal an unexpected association of m2 macrophages with oral cancer free survival. *OncoImmunology*, 10(1):1944554, 2021.

[4] Ishida et al. Induction of unique macrophage subset by simultaneous stimulation with lps and il-4. *Frontiers in Immunology*, 14:1111729, 2023.

[5] Warnakulasuriya et al. Nomenclature and classification of potentially malignant disorders of the oral mucosa: potentially malignant disorders. *J Oral Pathol Med*, 36:575–580, 2007.

[6] Dionne et al. Potentially malignant disorders of the oral cavity: Current practice and future directions in the clinic and laboratory. *International journal of cancer*, 136(3):503–515, 2015.

[7] Hanahan. Hallmarks of cancer: New dimensions. *Cancer Discovery*, 12(1):31–46, 2022.

[8] Clairambault et al. A phenotype-structured model for the tumour-immune response. *Mathematical modelling of natural phenomena*, 18:22, 2023.

[9] Alvarez et al. Evolution of a structured cell population endowed with plasticity of traits under constraints on and between the traits. *Mathematical Biology*, 85(64), 2022.

[10] Perthame. *Transport Equations in Biology*. Birkhäuser Basel, Basel, 1st edition, 2007.

[11] Hirsch. Systems of differential equations which are competitive or cooperative: I. limit sets. *SIAM Journal on Mathematical Analysis*, 13(2):170, 1982. Web.

[12] Trélat et al. Pouchol, Clairambault. Asymptotic analysis and optimal control of an integro-differential system modelling healthy and cancer cells exposed to chemotherapy. *J. Maths Pures Appl.*, 116(9):268–308, 2018.